 doi:10.20944/preprints201904.0041.v1

Reproduction of Local Strong Wind Area Induced in the Downstream of Small-scale Terrain by Computational Fluid Dynamic (CFD) Approach

Takanori Uchida*
Research Institute for Applied Mechanics (RIAM), Kyushu University, 6-1 Kasuga-kouen, Kasuga, Fukuoka 816-8580, Japan
*Correspondence author; E-Mail: takanori@ riam.kyushu-u.ac.jp; Tel.: +81-92-583-7776; Fax: +81-92-583-7779.

Keiji Araki
Meteorological Disaster Prevention Group Railway Technical Research Institute (RTRI), 2-8-38 Hikari-cho, Kokubunji, Tokyo, 185-8540, JAPAN

Abstract

In this research, the computational fluid dynamic (CFD) approach that has been used in wind power generation field was applied for the solution of the problems of local strong wind areas in railway fields, and the mechanism of wind generation was discussed. At the same time, the affectivity of the application of computational fluid dynamic approach to railway field was discussed. The problem of local wind that occurs on the railway line in winter was taken up in this research. A computational simulation for the prediction of wind conditions by LES was implemented and it was clarified that the local strong wind area is mainly caused by separated flows originating from the small-scale terrain positioned at its upstream (at approximately 180.0 m above sea level). Meanwhile, the effects of the size of calculation area and spatial grid resolution on the result of calculation and the effect of atmospheric stability were also discussed. It was clarified that when the air flow characteristic of the separated flow originating from the small-scale terrain (at altitude of approximately 180.0 m) targeted in this research is reproduced at high accuracy by computational simulation of wind conditions, approximately 10.0 m of spatial resolution of computational grid in horizontal direction is required. As a result of the computational simulation of wind conditions of stably stratified flow (Fr = 1.0), lee waves were excited at the downstream of the terrain over time. As a result, the reverse-flow region lying behind the terrain that had been observed at a neutral time was inhibited. Consequently, local strong wind area was generated at the downstream of the terrain and the strong wind area passing through the observation mast was observed. By investigating the speed increasing rate of local strong wind area induced at the time of stable stratification, it was found that the wind was approximately 1.2 times stronger than what was generated at a neutral time.

Keywords: Terrain-induced severe wind event, Stratified flows, Computational Fluid Dynamics (CFD), LES

1. Introduction

At present, wind power generation business is rapidly growing at an unprecedented rate around the world. This is due to it being the best in cost performance in order to attain the nonuse of fossil fuel and the reduction of CO2 generation among renewable energies. In Japan as well, wind power generation is the leading source of renewable energy, so that further prevalence of wind power generation throughout the world would surely contribute to the overcoming of global warming (green innovation). One of the technical problems in the field of wind power generation to be solved in the future is to correctly understand local wind conditions which generate around wind turbines and establish a computational wind prospecting technology with higher accuracy than before that can be applied to the survey before the introduction of wind turbines [1–11]. The author's group narrowed down the scales from several m to several km and is developing a computational wind prospecting model that can reproduce local wind conditions generated there in high accuracy (RIAM-COMPACT) [12–33]. By employing LES (Large-Eddy Simulation) for the turbulence model, it becomes possible to reproduce non-steady wind conditions that change temporally and spatially.

Recently, the accidents of wind turbines of onshore wind farms constructed on complex trains in mountainous regions are rapidly increasing. According to a recent survey conducted by the author et al., it has been pointed out

Preprints (www.preprints.org) | NOT PEER-REVIEWED | Posted: 3 April 2019 doi:10.20944/preprints201904.0041.v1

that these accidents of wind turbines are strongly related to topographic turbulence (turbulent flow field originating from terrain). In addition to the problem of topographic turbulence, as above mentioned, multiple large-scale wind turbines which are intensively constructed in mountainous regions for onshore wind farms are actual situations in Japan which cannot be helped. Therefore, in order to prevent the lowering of the entire amount of electric power generated in a wind farm caused by mutual intervention of each wind turbine, the development of a wake model that determines appropriate distance between wind turbines has become the most important subject of the future tasks. In the case of offshore wind farms which have been drawing attention, the problem of the distance between wind turbines, i.e. the most appropriate arrangement of wind turbines, has become apparent.

In this research, a computational fluid dynamic approach that has been applied to the field of wind power generation was applied to the problem of local strong wind area in railway fields, and its generation mechanism was discussed. In tandem, the effectivity of the application of computational fluid dynamics approach to railway field was discussed. The field of railways has also had problems with strong wind that occurs along railway tracks [34–40]. More than 50 cases of accidental derailing and rollover caused by strong wind have been recorded in Japan, including one that occurred on the present Tokaido Line in 1889 (Meiji 22). The measures against strong wind in the railway fields mainly consist of structural measures (improvement of windbreak fence) and non-structural measures (operating rules). These measures have been developed through the lessons of these accidents. At present, strong wind monitoring along the railways is conducted by instantaneous wind speed observed by an anemometer. This is because the investigation of accidental derailing and rollover on the Sanin Main Line that occurred in 1986 verified that what greatly affects the accidents is instantaneous wind speed.

The railways in Japan thread through narrow and steep terrain and their railway environments also variously change from country area to city area to mountain area. In the downwind region of complex terrain, in particular, once strong winds occur, the intensifications of wind caused by topographic effect and topographic turbulence are feared. In order to prevent trains from the accident of derailing and rollover, it is important to linearly evaluate strong wind that occurs in the environment along railway track by instantaneous wind speed; however, for that purpose, it is not enough only to measure the wind along railways using an anemometer, the analysis of non-steady wind condition by CFD is also required.

In this research, the problem of local strong wind which occurs on the railway line in winter was taken up. On the railway line, the problems of the delays of trains at the time of strong wind in winter are often discussed. Against these problems, the characteristics of wind conditions of local strong wind areas generating around the railway line were discussed based upon the measured data for the first, and the weather GPV data. The direction of wind generating in strong wind areas, in particular, was estimated. After that, wind conditions in the narrow space of several dozen km or less were reproduced using computational wind prospecting technology (RIAM-COMPACT), and the mechanism of local strong wind generation was discussed. At the same time, the effects of the size of calculation area and spatial grid resolution on the result of calculation were also discussed. Finally, the effect of atmospheric stability was discussed.

2. Wind Conditions Characteristics of Local Wind Conditions by Measured Data and Weather GPV data

Figure 1 shows the locations of the railway line and observation mast, and the evaluation points of the weather GPV data in the neighborhood of observation mast. For measuring data, only a wind speed sensor was installed at the top of the observation mast, 5 m above ground, but no wind direction sensor was installed. The period of data recording was nine months from July 2014 to March 2015. For the verification of these measured data, LFM_S (Local Forecast Mode: S means surface data), which are weather GPV (Grid Point Value data) at 10 m above ground with spatial resolution of 2 km, provided by Japan meteorological Agency, was used. In this research, the weather GPV data at the point (longitude 130.15 degrees and latitude 33.52 degrees) nearest to the observation mast (longitude 130.1503333 degrees and latitude 33.5245 degrees) were used. The horizontal distance between the points of observation mast and weather GPV data was approximately 500 m.

Figure 2 shows the time variations (one-hour time interval) of wind speed and wind direction during the entire period of collecting data (nine months from July 2014 to March 2015). Regarding wind speed, the measured data (5 m above ground) are shown in a red line, and weather GPV data (10 m above ground) are shown in a blue line, both in the same graph. Regarding the wind direction corresponding to the above, because there are no measured

Preprints (www.preprints.org) | NOT PEER-REVIEWED | Posted: 3 April 2019 doi:10.20944/preprints201904.0041.v1

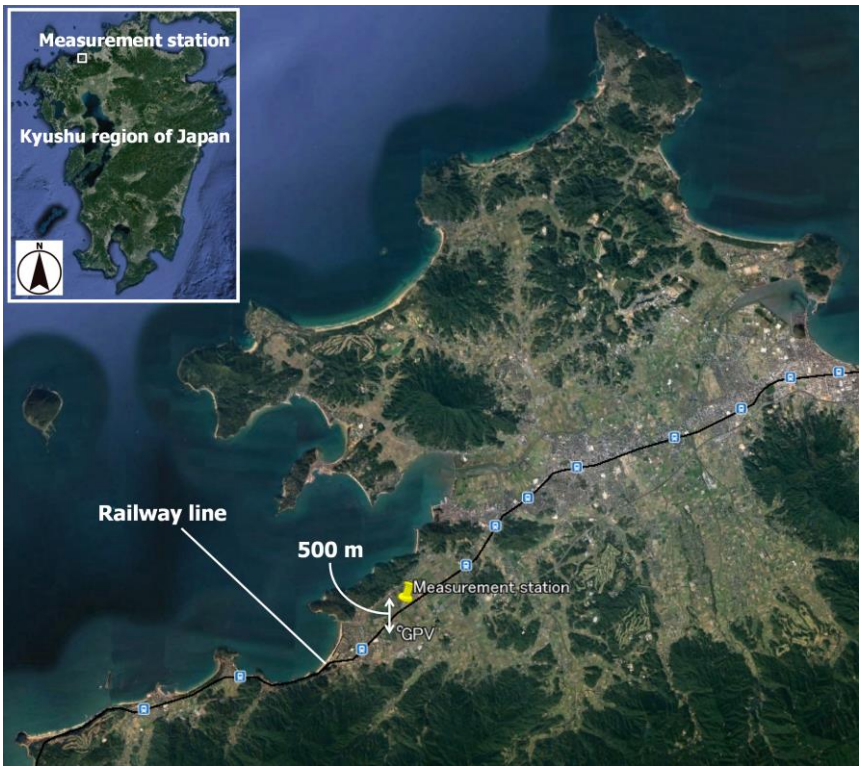

Figure 1 Locations of the railway line and observation mast, and evaluation points of weather GPV data existing around the observation mast

data, only weather GPV data are shown. As the result of the comparison between the wind speeds of measured data and those of weather GPV data, no large variations are observed in the reproduction of weather GPV data; however the variations in association with daily wind speed variation are well reproduced. Figure 3 shows the daily variations of wind speed and wind direction during the period from December 2014 to January 2015 as a sample of the data in the winter. As described in Figure 2, the comparison of wind speed shows that no large variations are observed in the reproduction of weather GPV data (10 m above ground) as observed in measured data (5 m above ground); however the variations in association with daily wind speed are well reproduced. As will be explained later in detail, it can be understood that the appearance frequency of wind direction (shown in red frame) in the north-northwest (defined angles clockwise between 281.25 degrees or more, and less than 303.75 degrees) is high. Figure 4 shows a scatter plot relating to the wind speed data of the measured data and weather GPV data. The correlation coefficient is approximately 0.09, which shows that there is a strong correlation between the measured data (5 m above ground) and weather GPV data (10 m above ground). As there is a strong correlation between the wind speeds of both data, the wind data of the weather GPV were used as the wind direction data corresponding to measured data in this research. A wind rose (nine months for whole period for data collected from July 2014 to March 2015) is shown in Figure 5, anew, in which the time-series data set consisting of the measured data (5 m above ground) and corresponding wind direction of weather GPV data (10 m above ground) was evaluated. As described in Figure 3, closer scrutiny of this figure showed that the appearance frequency of the wind from the west-northwest was extremely high, and it was defined as the main wind direction of this area. Based on the result of the analysis of Figure 5, all data falling under the wind direction range of the west-northwest were consecutively arranged in the time direction, as shown in Figure 6. There were 773 data falling under the wind direction rage of west-northwest, and they accounted for approximately 12% of all data. The average wind speed of 773 data was approximately 8.7 m/s, and the corresponding turbulence intensity was 57%; it was clarified that both showed great values. From the above result, it was quantitatively shown that when the winds from west-northwest blew in this area, local strong wind area was generated. In the next section, a computational simulation of wind conditions targeting the wind from west-northwest by LES will be conducted and the generation mechanism of local strong wind area will be discussed in detail.

Preprints (www.preprints.org) | NOT PEER-REVIEWED | Posted: 3 April 2019 doi:10.20944/preprints201904.0041.v1

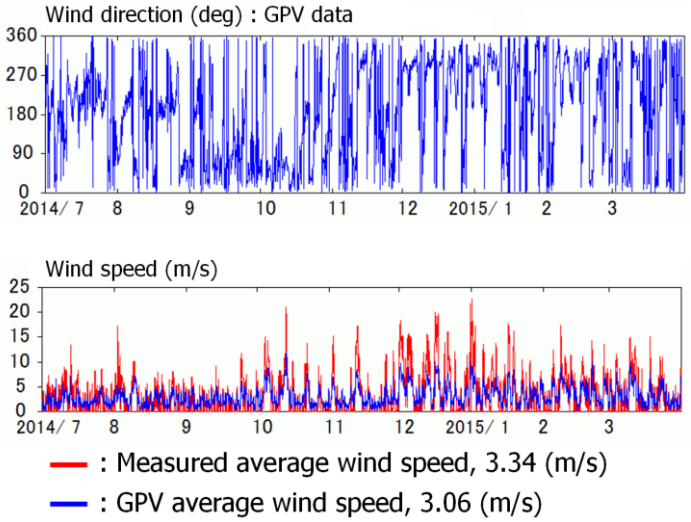

Figure 2 Comparison of measured data (5 m above ground) and weather GPV data (10 m above ground) for nine months from July 2014 to March 2015

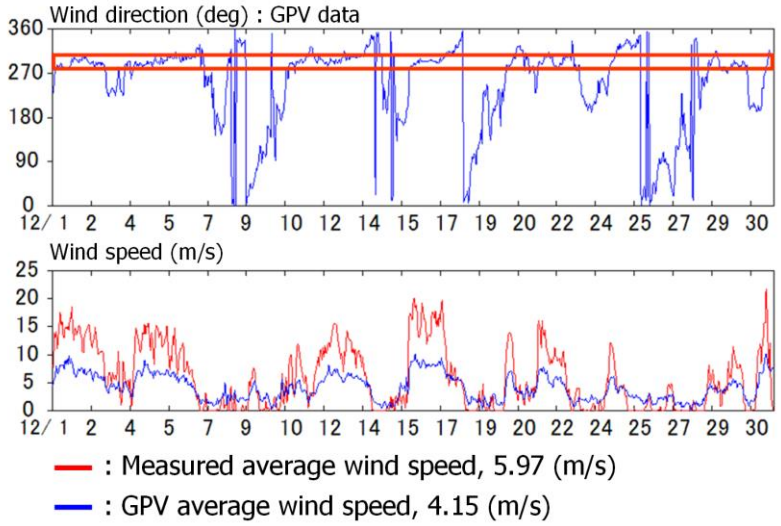

(a) December 2014

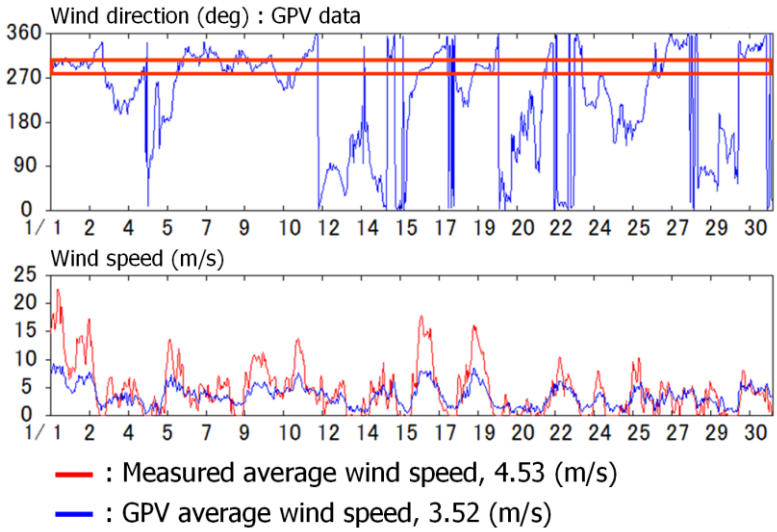

(b) January 2015

Figure 3 Comparison of measured data (5 m above ground) and weather GPV data (10 above ground) in December 2014 and January 2015

Preprints (www.preprints.org) | NOT PEER-REVIEWED | Posted: 3 April 2019 doi:10.20944/preprints201904.0041.v1

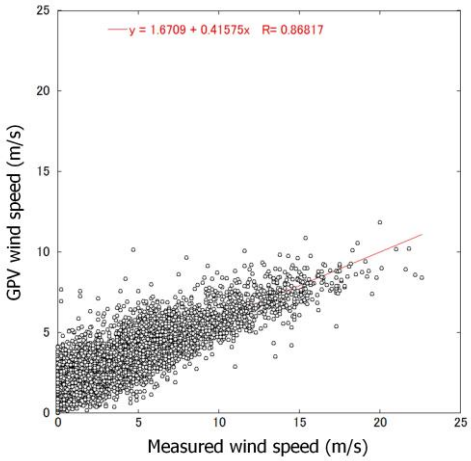

Figure 4 Scatter plot of measured data (5 m above ground) and weather GPV data (10 m above ground) for nine months from July 2014 to March 2015

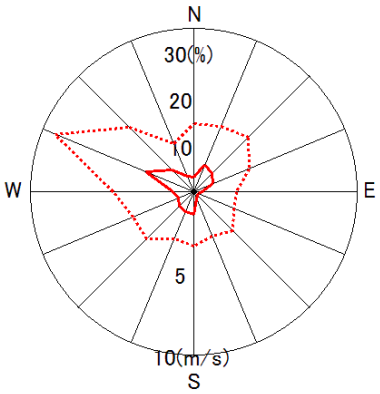

Figure 5 Wind rose for nine months from July 2014 to March 2015
Average wind speeds by wind direction (solid line) by measured data and wind direction appearance frequency (dotted line) by weather GPV data

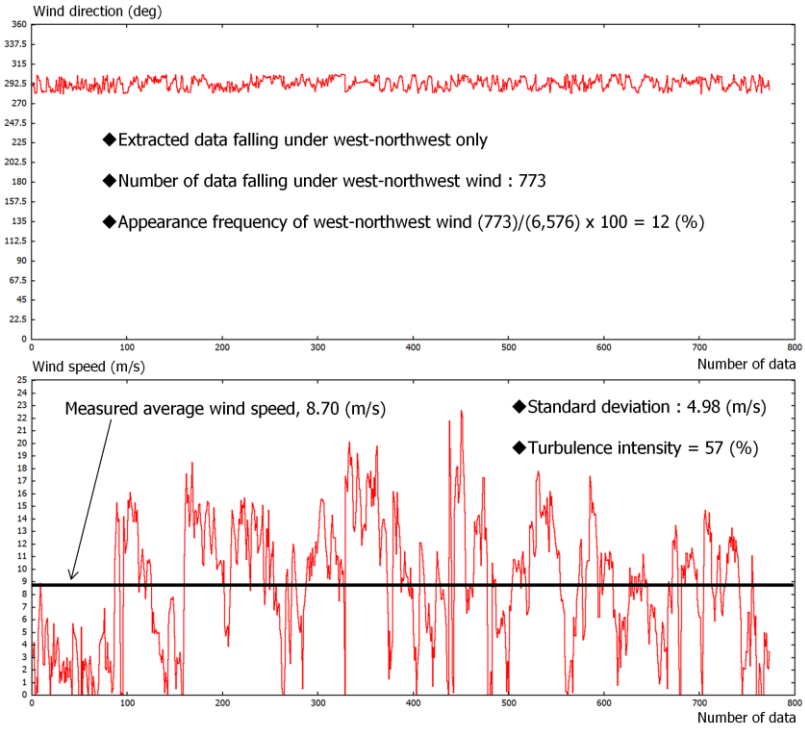

Figure 6 Wind speed data falling under west-northwest (defined angles clockwise between 281.25 degrees or more, and less than 303.75 degrees), consecutively arranged in time direction

Preprints (www.preprints.org) | NOT PEER-REVIEWED | Posted: 3 April 2019 doi:10.20944/preprints201904.0041.v1

3. Outline of Numerical Calculation Technique

In this research, in order to avoid numerical instability and predict the local flow of wind on the complex terrain in high accuracy, a collocated grid of generalized curvilinear coordinate system was used. Regarding the numerical calculation technique, based upon the finite-difference method (FDM), a large-eddy simulation (LES) was employed as turbulence model. In the case of LES, a spatial filter is provided in the flow field and the grid scale (GS) eddies larger than computational grid and sub-grid scale (SGS) eddies smaller than GS eddies are separated from the turbulent flow eddies of various sizes. GS large eddies are numerically simulated directly, not depending upon physical model. Meanwhile, energy dissipation action carried out by SGS small eddies was modeled mainly based on physical consideration of SGS stress. Please refer to past literature for the detailed calculation method.

The calculating area in this research has a space of 12.3 (x) × 3.5 (y) × 0.65 (z) km, in the main stream direction (x), right angle direction to mainstream (y) and vertical direction (z). The maximum altitude in the calculating area was 180.0 m, and the minimum latitude was 0.0 m. A 3D shape of the complex terrain was reproduced based upon the data of spatial resolution 10 m of the Geospatial Information Authority of Japan. The number of computational grids was approximately 18 million of the total number of 1,231 (x) × 351 (y) × 41 (z) in each direction. The grid widths to the x direction and y direction were assumed to be 10 m at uniform intervals. The grid width was non-uniform in the z direction so that the density of grid points increased smoothly toward the ground surface (Δz_{min} = 0.5 m). The targeted wind direction in this area for the research was presumed to be west-northwest, the main wind direction in this area as aforementioned. Regarding boundary conditions, a wind speed distribution following power law (N-value = 20) was applied to inlet boundary surface. Sliding condition was applied to side boundary surface and upper boundary surface and convective outflow condition was applied to outflow boundary surface. Adhesive condition was applied to ground surface. The Reynolds number, a dimensionless parameter, was assumed to be $Re = 10^4$ in this simulation and dimensionless time step to be 0.002.

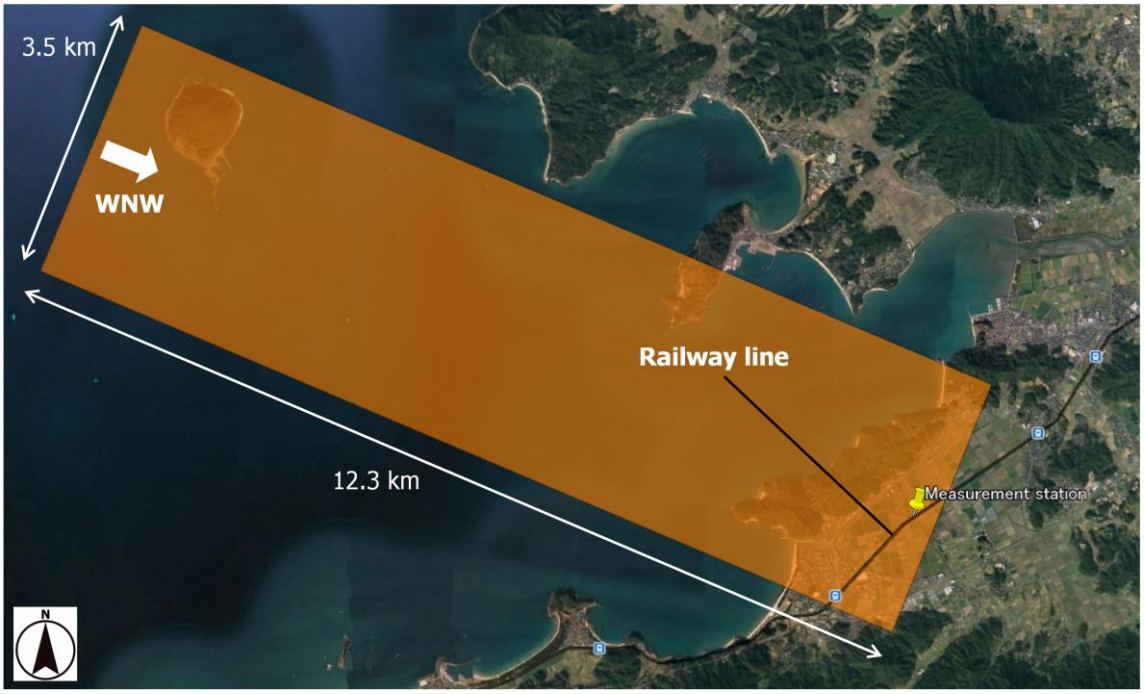

Figure 7 Calculation area and others

4. Calculation Result and Discussion

Figure 8 shows the wind speed distribution in the direction of the mainstream (x) (instantaneous flow field, horizontal cross-section 5 m above ground), the result of computational simulation of wind conditions, projected into Google Earth. It can be observed that the neighborhood of observation mast is strongly affected by separated flow (complex turbulent field) originating from small-scale terrain positioned at the side of the upstream (at an altitude of approximately 180.0 m).

Preprints (www.preprints.org) | NOT PEER-REVIEWED | Posted: 3 April 2019 doi:10.20944/preprints201904.0041.v1

Figure 9 shows a wind speed distribution (instantaneous flow field, vertical cross-section passing observation mast) in the mainstream direction. From this figure also, it can be known that the neighborhood of observation mast is directly affected by a separate flow originating from the small-scale terrain (at altitude of approximately 180.0 m) positioned nearby upstream. In particular, a separated flow originating from the small-scale terrain adheres to the ground; along with that, a very strong wind area is locally formed, and it can be observed that it passes through the observation mast (the area boxed with black lines in the figure).

Figure 10 shows the time variation of the wind direction (angle) within the horizontal cross-section of the wind passing through the observation mast (5 m above ground). In this figure, two red lines are drawn showing ± 25 degrees. By scrutinizing this figure, it can be observed that changes in wind direction over 25 degrees in the horizontal direction often occur, which suggests that this exerts a large wind load on trains. The prediction of the occurrence of non-steady wind load and the countermeasure for it will become further important in the future from viewpoint of safe operation of trains.

Figure 11 shows the time variation of the wind speed by computational simulation of wind conditions (5 m above ground). The values were converted so that the average value of wind speeds equals that obtained from the measured values (approximately 8.7 m/s) shown in Figure 6. Focusing on the time history waveform of wind speed, it was shown that large airflow changes occur simultaneously in the measured data of Figure 6. As a result, the turbulent intensity calculated from computational simulation of wind conditions also showed very large values (approximately 32 %) similar to the measured data. From the above results, it was suggested that the very large turbulence intensity (approximately 57 %) obtained from the measured data of Figure 6 was mainly caused by separated flow originating from a small-scale terrain (at latitude of approximately 180.0 m) positioned at the upstream site.

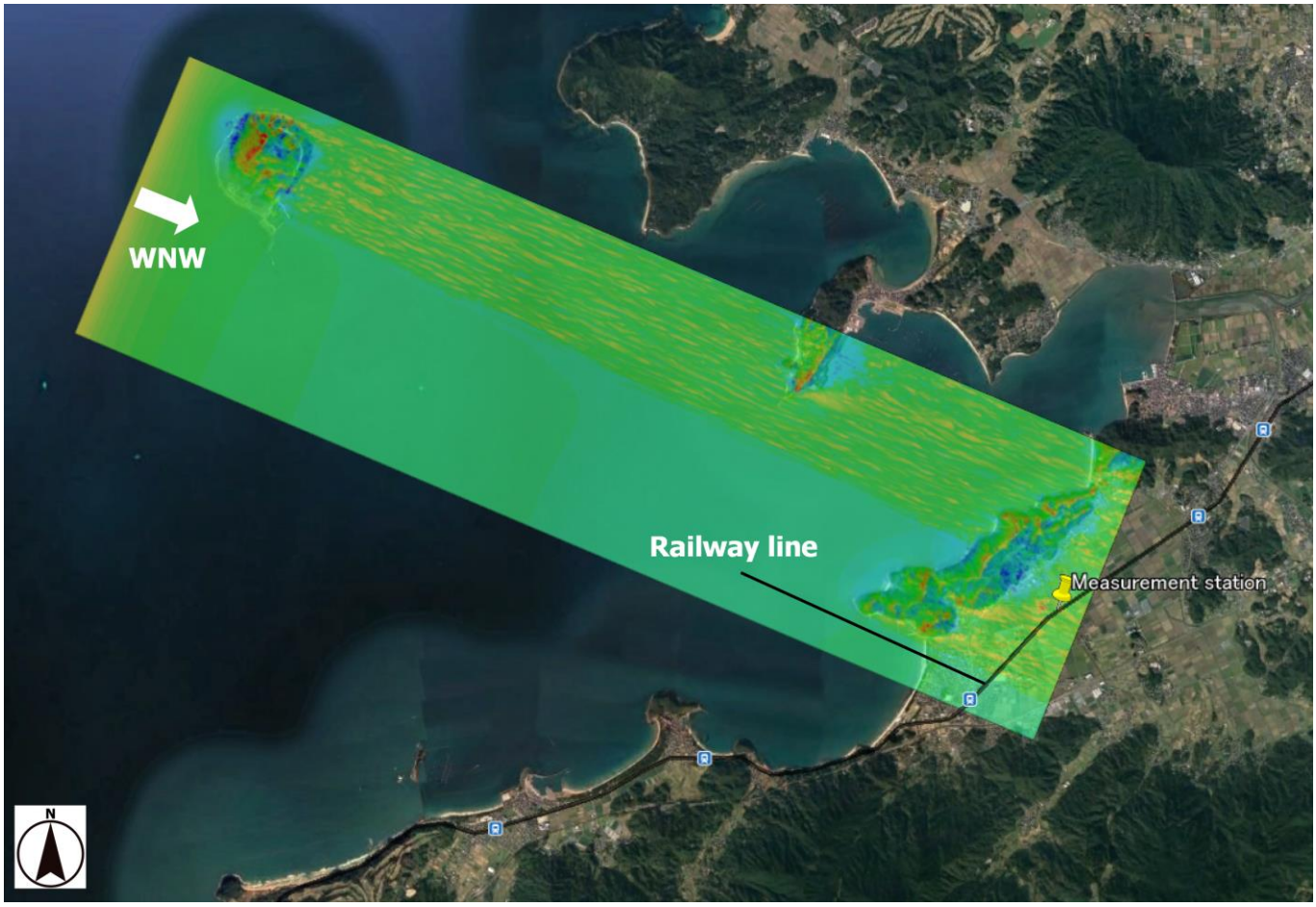

Figure 8 Wind speed distribution in the mainstream direction (x), instantaneous flow field and horizontal cross-section 5 m above ground

Preprints (www.preprints.org) | NOT PEER-REVIEWED | Posted: 3 April 2019 doi:10.20944/preprints201904.0041.v1

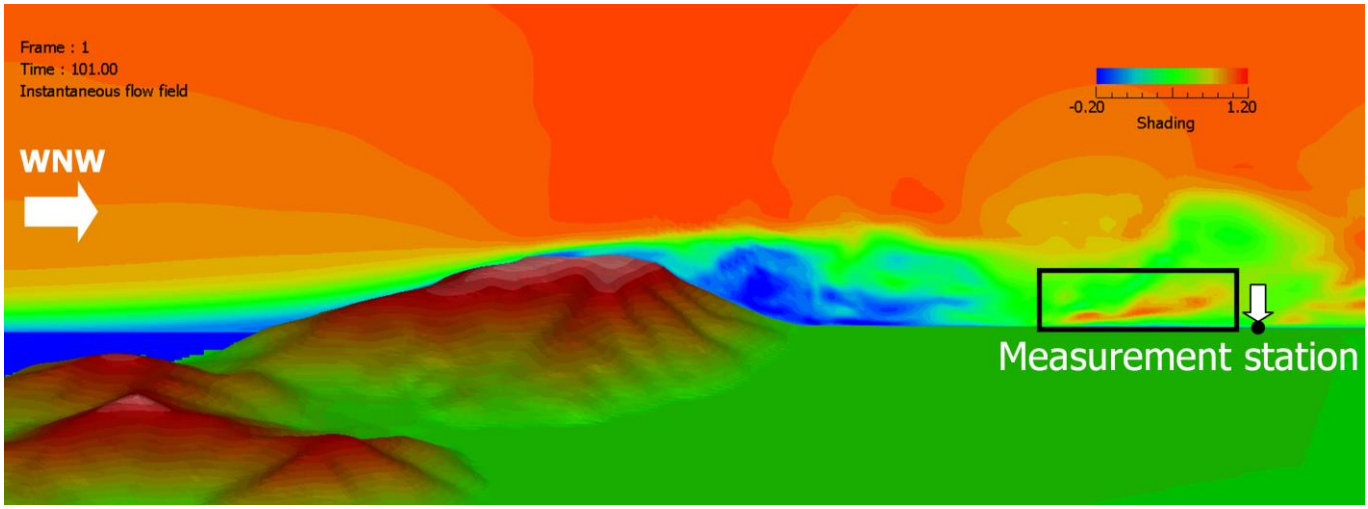

Figure 9 Wind speed distribution in the mainstream direction (x), instantaneous flow field and vertical cross-section passing through observation mast

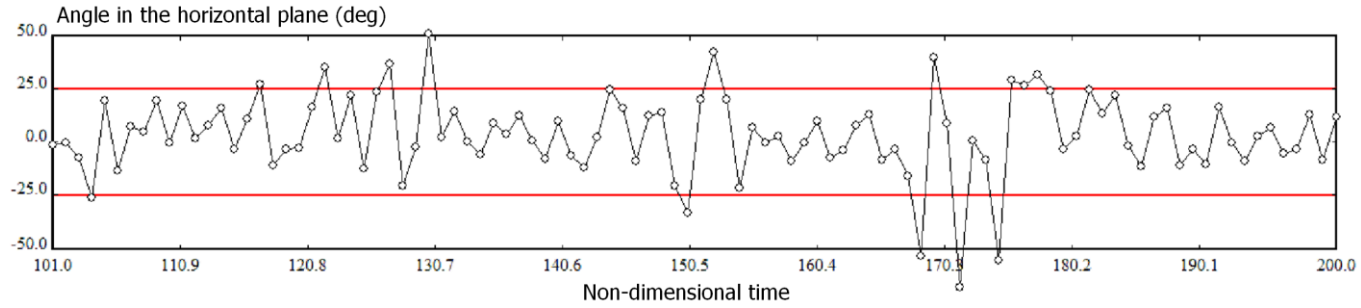

Figure 10 Time variation of wind direction (angle) within horizontal cross-section of the wind passing through the observation mast, 5 m above ground.

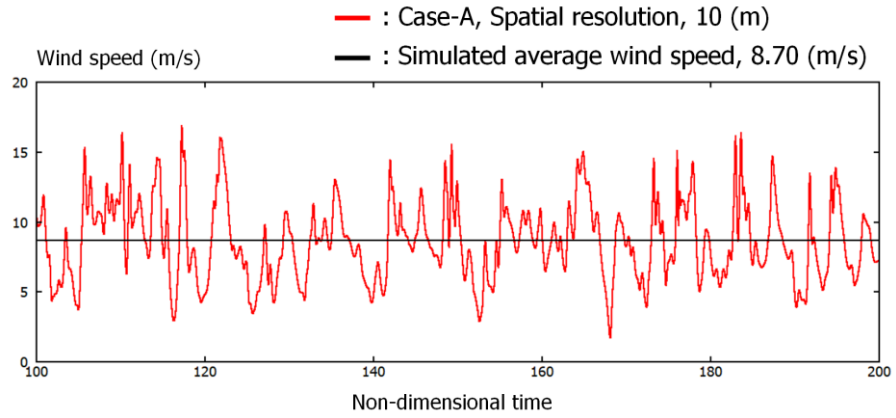

Figure 11 Time variation of wind speed by computational simulation of wind conditions, spatial resolution 10 m, 5 m above ground.

5. Effects of Size of Calculation Area and Grid Resolution in the Horizontal Direction

Computational simulations of wind conditions were implemented by changing the size of the calculation area and grid resolution in the horizontal direction, and the effects of these calculation parameters on the accuracy of reproduction of the area of local wind conditions were discussed. As Figure 12 shows, a space of 3.0 (x) × 2.5 (y) × 0.65 (z) km in the mainstream direction (x), right angle direction to mainstream (y) and vertical direction (z) was set up for calculation area. The size of the area in the z direction is the same as that of Figure 7, and the maximum altitude (180.0 m) and the minimum altitude (0.0 m) in the calculation area also are the same as those of Figure 7. The terrain altitude data were also based upon those of spatial resolution 10 m of the Geospatial Information

Preprints (www.preprints.org) | NOT PEER-REVIEWED | Posted: 3 April 2019 doi:10.20944/preprints201904.0041.v1

Authority of Japan. Regarding the computational grids, the grid widths in the x direction and y direction were assumed to be as large as two times the spatial resolution of Figure 7, at uniform intervals of 5 m. The grid width was non-uniform in the z direction so that the density of grid points increased smoothly toward the ground surface. The minimum grid width in the vertical direction was 0.5 m, similar to that of Figure 7. The total number of computational grids was approximately 12 million of 601 (x) × 501 (y) × 41 (z) in each direction. Associated with the increase of the grid resolution at horizontal direction, dimensionless time step was set to 0.0001. Other initial conditions and boundary conditions were as the same as those of the computational simulation of wind conditions, as mentioned previously.

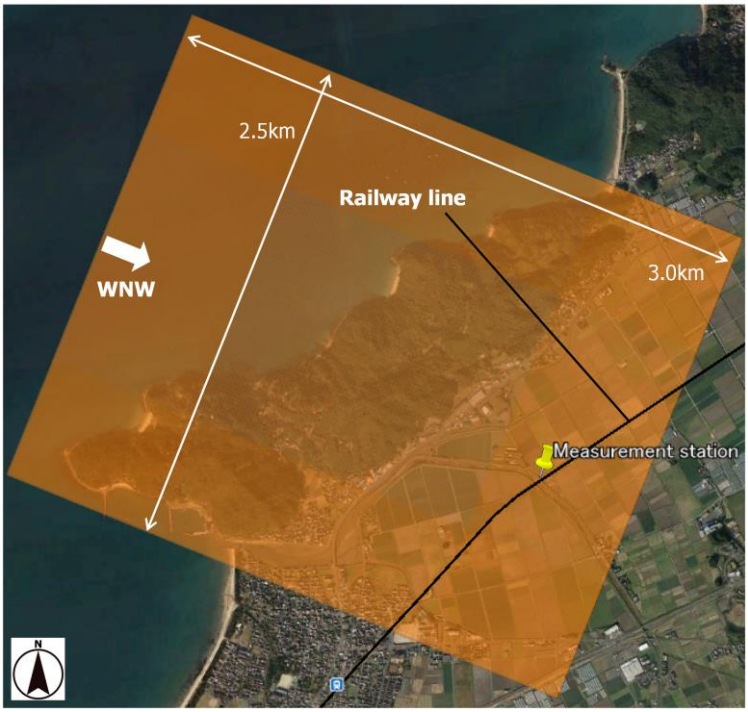

Figure 12 Calculation area when grid resolution in the horizontal direction was increased

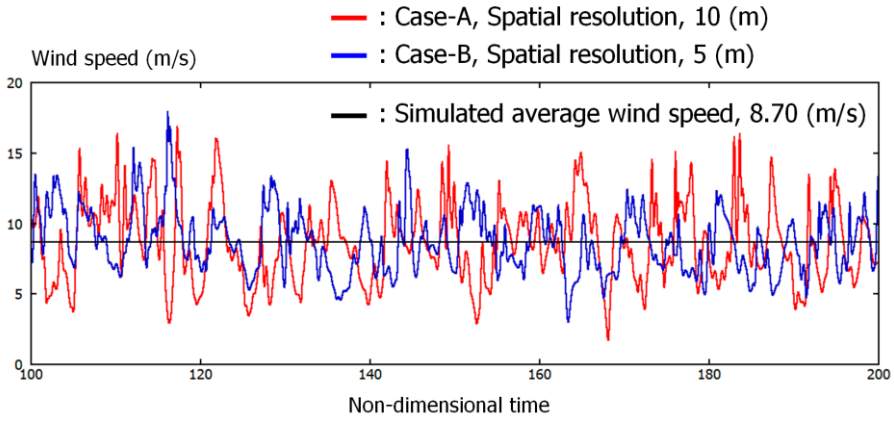

Figure 13 Time variation of wind speed in computational simulation of wind conditions and comparison of spatial resolution 10 m and 5 m at 5 m above ground

Figure 13 shows the comparison of time variations of wind speed at resolutions of 10.0 m and 5.0 m (at 5 m above ground). The values were converted so that the average value of wind speed (dimensionless quantity) were equal to that obtained from the measured values (approximately 8.7 m/s) shown in Figure 6. Focusing on the time history of waveform, no significant difference was observed between the calculation results at spatial resolutions

Preprints (www.preprints.org) | NOT PEER-REVIEWED | Posted: 3 April 2019 doi:10.20944/preprints201904.0041.v1

10.0 m and 5.0 m. Regarding turbulent intensity, approximately the same result was obtained. From the above, it was clarified that, when the air flow characteristics of separated flow originating from the small-scale terrain targeted in this research (at an altitude of approximately 180.0 m) is reproduced in high accuracy, the spatial resolution of computational grids in the horizontal direction needs to be approximately 10.0 m.

6. Effect of Atmospheric Stability

Generally, atmospheric boundary layer has a stratified state where the concentration of density (or temperature) changes in the vertical direction, and the flow in the ground inversion layer, which often occurs at night, forms a sable satisfied flow where the concentration of density decreases at higher altitudes (temperature becomes high). It is known that when the stably stratified flows pass through ground structures, simple terrain or complex terrain, a negative buoyancy acts on the flow field and various wave phenomena and flow phenomena occur. The wave phenomena and flow phenomena that occur at stably stratified fields are related to topographic strong wind disaster (local strong wind disaster) and they are important issues as the environmental problems at the time of strong wind. In the region targeted in this research, air currents passing above sea during winter invaded into a small-scale terrain (at an altitude of approximately 180.0 m), so that the safely stratified state should be considered. Therefore, in this research, the author et al. focused on atmospheric stability where lee waves(internal gravity wave) were excited at the side of downstream of a small-scale terrain (at an altitude of approximately 180.0 m) and discussed the speed increasing rate of local strong wind areas which were induced. Speed increasing rate = (Average value of wind speed at the time of stable stratification at 5 m above ground)/(average value of wind speed at the neutral time; averaging time is dimensionless time 10.0) The dimensionless parameter relating to atmospheric stability used in this research is Froude number (= U/Nh). Here, U is wind speed, h is the height of terrain, and N is buoyancy frequency.

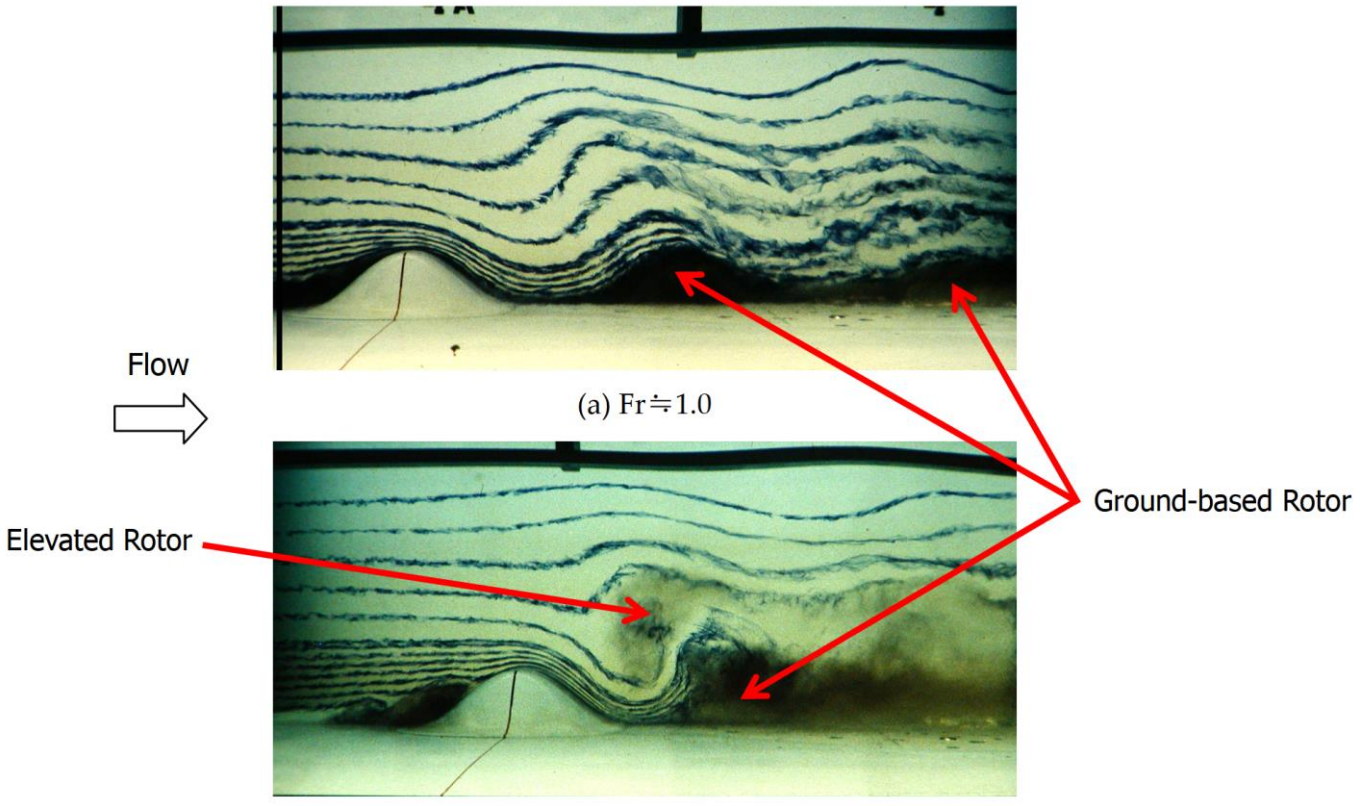

Figure 14 Result of visualization using towing water tank (William H. Snyder [41])

Preprints (www.preprints.org) | NOT PEER-REVIEWED | Posted: 3 April 2019 doi:10.20944/preprints201904.0041.v1

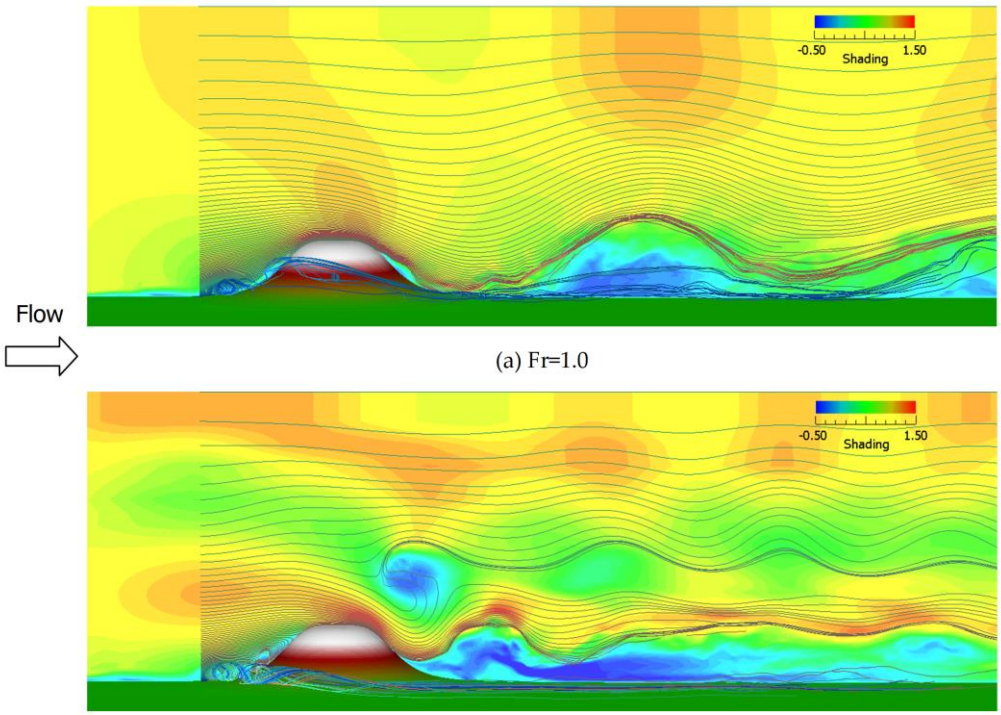

Figure 15 Result of visualization by computational simulation of wind conditions, Re =10^4

Figure 14 shows the result of visualization of the stably stratified flows (Fr ≒ 1.0 and 0.5) moving beyond isolated peaks visualized by using the towing water tank. In Figure 14 (a), lee waves of long wavelengths are formed in the downstream of the terrain, and at the same time, ground-based rotors are formed close to the ground. In Figure 14 (b), where the flows were more stably stratified, the wave lengths of lee wave become short and at the same time, it can be observed that an elevated rotor is formed above the downstream of the terrain corresponding to the ground-based rotors.

Figure 15 shows the result of the computational simulation of wind conditions (instantaneous flow field, Fr = 1.0 and 0.5) conducted under similar conditions as Figure 14, as shown above. Figure 15 shows a streamline view drawn as the trajectories of visual particles released from the upper stream of the terrain and the distribution of wind speeds in the mainstream direction (x). A review of Figure 15 shows that the wave patterns, ground-based rotors and elevated rotor obtained by the water-tank experiment are reproduced there, and it was confirmed that the computational simulation program of wind conditions reproduced very well the stably stratified flows passing through the terrain. From the above, it was determined to apply this program to actual complex terrains.

Figure 16 shows the result of computational simulation of wind conditions of stably stratified flows (Wind direction is WNW, Fr = 1.0) conducted targeting the calculation area shown in Figure 12 (grid resolution 5 m in horizontal direction). Figure 16, here, shows the time variation in wind condition area at dimensionless time interval 2.5. Lee waves are excited at the downstream of the terrain over time. Additionally, the reverse-flow region lying behind the terrain that had been observed at the neutral time in Figure 9 is inhibited. As a result, in the downstream of the terrain, a local strong wind area occurs as pointed out by arrow, and the strong wind area passing through the observation mast can be observed. The increasing rate of speed in the local strong wind area induced under stable stratification was discussed and it was clarified that wind approximately 1.2 times as strong as that at neutral time was generated. The speed increasing rate = (Average wind speed value under stable stratification at 5 m above ground) / (average value of wind speeds at neutral time, averaging time is dimensionless time 10.0)

Preprints (www.preprints.org) | NOT PEER-REVIEWED | Posted: 3 April 2019 doi:10.20944/preprints201904.0041.v1

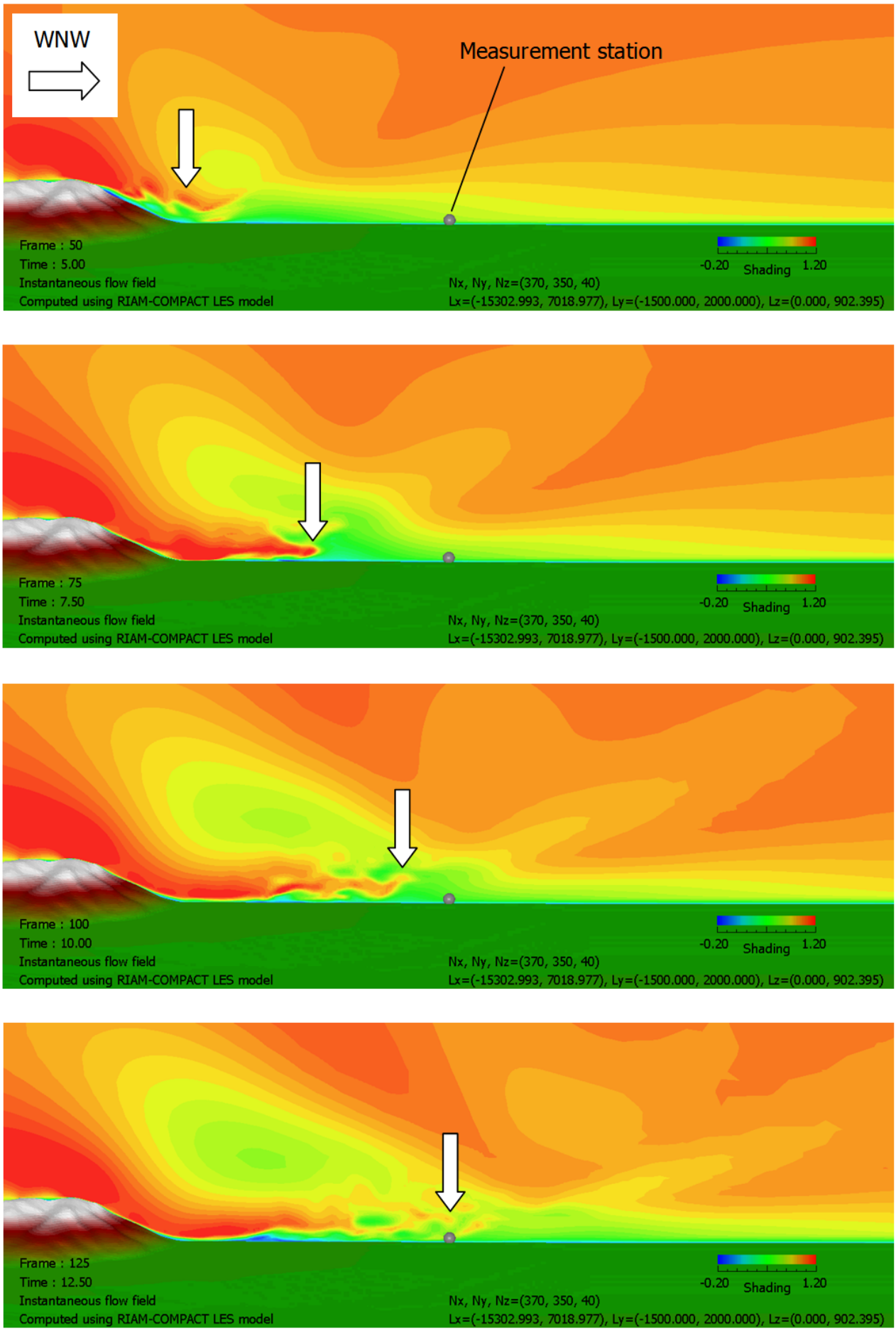

Figure 16 Result of computational simulation of wind conditions of stably stratified flow targeting actual complex terrain

7. Conclusions

In this research, a computational fluid dynamics (CFD) approach that has been used in wind power generation fields was applied as a solution for the problems of local strong wind areas in railway fields. The mechanism of wind generation was discussed, and at the same time, the effectiveness of its application to railway field was discussed. The problem of strong local wind that occurs in the railway line in winter was taken up in this research. In the railway line, train delays at the time of strong winds in the winter often causes problems. Against this problem, the characteristics of wind conditions of local strong wind area generating around the railway line were discussed based upon the measured data for the first, and the weather GPV data. As the result of the investigation, it was shown that the direction of this strong wind was west northwest. Then, a computational simulation of wind conditions targeting this wind from the west northwest by LES was implemented and it was clarified that the local strong wind area was mainly caused by the separated flow originating from a small-scale terrain (at an altitude of approximately 180.0 m) positioned at the side of its upstream. And, at the time, the effects of the size of calculation area and spatial grid resolution on the result of calculation and the effect of atmospheric stability were also discussed. It was clarified that when the air flow characteristic of the separated flow originating from the small-scale terrain (at altitude of approximately 180.0m) targeted in this research is to be reproduced at a high accuracy by computational simulation of wind condition characteristics, approximately 10.0 m of spatial resolution of computational grid in the horizontal direction is required. As a result of the computational simulation of wind conditions of the stably stratified flow (Fr = 1.0), lee waves were excited at the downstream of the terrain over time. As a result, the reverse-flow region lying behind the terrain that had been observed at the neutral time was inhibited. This generated a local strong wind area at the downstream of the terrain, and the strong wind area passing through the observation mast was observed. The investigation of the increasing rate of speed of the local strong wind area induced at the time of stable stratification showed that wind approximately 1.2 times as strong as that at neutral time was generated. The speed increasing rate = (Average wind speed value under stable stratification at 5 m above ground)/(average value of wind speed at neutral time, averaging time is dimensionless time 10.0)

Acknowledgement

This research was supported by a joint research with Kyushu Railway Company, a research project assigned by West Japan Railway Company and a joint research project with Railway Technical Research Institute. We strongly appreciate the cooperation.

References

1. Rodrigues, R.V.; Lengsfeld, C. Development of a Computational System to Improve Wind Farm Layout, Part I: Model Validation and Near Wake Analysis. Energies 2019, 12, 940.
2. Abel Gargallo-Peiró, Matias Avila, Herbert Owen, Luis Prieto-Godino, Arnau Folch, Mesh generation, sizing and convergence for onshore and offshore wind farm Atmospheric Boundary Layer flow simulation with actuator discs, Journal of Computational Physics, Volume 375, Pages 209-227, 2018
3. Sessarego M, Shen WZ, Van der Laan MP, Hansen KS, Zhu WJ. CFD Simulations of Flows in a Wind Farm in Complex Terrain and Comparisons to Measurements. Applied Sciences. 2018; 8(5):788.
4. Orkun Temel, Laurent Bricteux, Jeroen van Beeck, Coupled WRF-OpenFOAM study of wind flow over complex terrain, Journal of Wind Engineering and Industrial Aerodynamics, Volume 174, Pages 152-169, 2018
5. Castellani, F.; Buzzoni, M.; Astolfi, D.; D'Elia, G.; Dalpiaz, G.; Terzi, L. Wind Turbine Loads Induced by Terrain and Wakes: An Experimental Study through Vibration Analysis and Computational Fluid Dynamics. Energies2017, 10, 1839.
6. K.S.R. Murthy, O.P. Rahi, A comprehensive review of wind resource assessment, Renewable and Sustainable Energy Reviews, Volume 72, Pages 1320-1342, 2017
7. Teresa Simões, Ana Estanqueiro, A new methodology for urban wind resource assessment, Renewable Energy, Volume 89, Pages 598-605, 2016
8. Harish Gopalan, Christopher Gundling, Kevin Brown, Beatrice Roget, Jayanarayanan Sitaraman, Jefferey D.

Mirocha, Wayne O. Miller, A coupled mesoscale-microscale framework for wind resource estimation and farm aerodynamics, Journal of Wind Engineering and Industrial Aerodynamics, Volume 132, Pages 13-26, 2014

9. T.F. Ishugah, Y. Li, R.Z. Wang, J.K. Kiplagat, Advances in wind energy resource exploitation in urban environment: A review, Renewable and Sustainable Energy Reviews, Volume 37, Pages 613-626, 2014
10. Porté-Agel, F.; Wu, Y.-T.; Chen, C.-H. A Numerical Study of the Effects of Wind Direction on Turbine Wakes and Power Losses in a Large Wind Farm. Energies 2013, 6, 5297-5313.
11. J.M.L.M. Palma, F.A. Castro, L.F. Ribeiro, A.H. Rodrigues, A.P. Pinto, Linear and nonlinear models in wind resource assessment and wind turbine micro-siting in complex terrain, Journal of Wind Engineering and Industrial Aerodynamics, Volume 96, Pages 2308-2326, 2008
12. Kenji ONO and Takanori UCHIDA, High-Performance Parallel Simulation of Airflow for Complex Terrain Surface, Modelling and Simulation in Engineering, Volume 2019, Article ID 5231839, 2019, DOI:https://doi.org/10.1155/2019/5231839
13. Takanori UCHIDA, Large-Eddy Simulation of Airflow over a Steep, Three-dimensional Isolated Hill with Multi-GPUs Computing, Open Journal of Fluid Dynamics, Vol.8, pp.416-434, 2018, DOI:https://doi.org/10.4236/ojfd.2018.84027
14. Takanori UCHIDA , Numerical Investigation of Terrain-induced Turbulence in Complex Terrain by Large-eddy Simulation (LES) Technique, Energies, 11(10), 2638, 2018, DOI:https://doi.org/10.3390/en11102638
15. Takanori UCHIDA and Graham Li, Comparison of RANS and LES in the Prediction of Airflow Field over Steep Complex Terrain, Open Journal of Fluid Dynamics, Vol.8, pp.286-307, 2018, DOI:https://doi.org/10.4236/ojfd.2018.83018
16. Takanori UCHIDA, Designed Wind Speed Evaluation Technique in Wind Turbine Installation Point by Using the Meteorological Model and CFD Model, Journal of Flow Control, Measurement & Visualization, Vol.6, pp.168-184, 2018, DOI:https://doi.org/10.4236/jfcmv.2018.63014
17. Takanori UCHIDA, Computational Investigation of the Causes of Wind Turbine Blade Damage at Japan's Wind Farm in Complex Terrain, Journal of Flow Control, Measurement & Visualization, Vol.6, pp.152-167, 2018, DOI:https://doi.org/10.4236/jfcmv.2018.63013
18. Takanori UCHIDA , Computational Fluid Dynamics Approach to Predict the Actual Wind Speed over Complex Terrain, Energies, 11(7), 1694, 2018, DOI:https://doi.org/10.3390/en11071694
19. Takanori UCHIDA, LES Investigation of Terrain-Induced Turbulence in Complex Terrain and Economic Effects of Wind Turbine Control, Energies, 11(6), 1530, 2018, DOI:https://doi.org/10.3390/en11061530
20. Takanori UCHIDA, Computational Fluid Dynamics (CFD) Investigation of Wind Turbine Nacelle Separation Accident over Complex Terrain in Japan, Energies, 11(6), 1485, 2018, DOI:https://doi.org/10.3390/en11061485
21. Takanori UCHIDA, A New Proposal for Vertical Extrapolation of Offshore Wind Speed and an Assessment of Offshore Wind Energy Potential for the Hibikinada Area, Kitakyushu, Japan, Energy and Power Engineering, Vol.10, pp.154-164, 2018, DOI:10.4236/epe.2018.104011
22. Takanori UCHIDA, Large-Eddy Simulation and Wind Tunnel Experiment of Airflow over Bolund Hill, Open Journal of Fluid Dynamics, Vol.8, pp.30-43, 2018, DOI:https://doi.org/10.4236/ojfd.2018.81003
23. Takanori UCHIDA , Three-Dimensional Numerical Simulation of Stably Stratified Flows over a Two-Dimensional Hill, Open Journal of Fluid Dynamics, Vol.7, pp.579-595, 2017, DOI:https://doi.org/10.4236/ojfd.2017.74039
24. Takanori UCHIDA, High-Resolution LES of Terrain-Induced Turbulence around Wind Turbine Generators by Using Turbulent Inflow Boundary Conditions, Open Journal of Fluid Dynamics, Vol.7, pp.511-524, 2017, DOI:https://doi.org/10.4236/ojfd.2017.74035
25. Takanori UCHIDA , CFD Prediction of the Airflow at a Large-Scale Wind Farm above a Steep, Three-Dimensional Escarpment, Energy and Power Engineering, Vol.09, pp.829-842, 2017, DOI:https://doi.org/10.4236/epe.2017.913052
26. Takanori UCHIDA, High-Resolution Micro-Siting Technique for Large Scale Wind Farm Outside of Japan Using LES Turbulence Model, Energy and Power Engineering, Vol.09, pp.802-813, 2017, DOI:https://doi.org/10.4236/epe.2017.912050
27. Takanori Uchida, Takashi Maruyama and Yuji Ohya, New Evaluation Technique for WTG Design Wind Speed

using a CFD-model-based Unsteady Flow Simulation with WindDirection Changes, Modelling and Simulation in Engineering, Volume 2011

28. Takanori Uchida and Yuji Ohya, Latest Developments in Numerical Wind Synopsis Prediction Using the RIAM-COMPACT® CFD Model, Energies, Vol.4, pp.458-474, 2011
29. Takanori Uchida and Yuji Ohya, Verification of the Prediction Accuracy of Annual Energy Output at Noma Wind Park by the Non-Stationary and Non-Linear Wind Synopsis Simulator, RIAM-COMPACT, Journal of Fluid Science and Technology, Vol.3, No.3, pp.344-358, 2008
30. Takanori Uchida and Yuji Ohya, Micro-siting technique for wind turbine generators by using large-eddy simulation, Journal of Wind Engineering & Industrial Aerodynamics, Vol.96, pp.2121-2138, 2008
31. Takanori Uchida and Yuji Ohya, Application of LES technique to diagnosis of wind farm by using high resolution elevation data, JSME International Journal 「Environmental Flows」, Series B, Vol.49, No.3, pp.567-575, 2006
32. Takanori Uchida and Yuji Ohya, Large-eddy simulation of turbulent airflow over complex terrain, Journal of Wind Engineering & Industrial Aerodynamics, Vol.91, pp.219-229, 2003
33. Takanori Uchida and Yuji Ohya, Numerical simulation of atmospheric flow over complex terrain, Journal of Wind Engineering & Industrial Aerodynamics, Vol.81, pp.283-293, 1999
34. Yayoi Misu, Takeshi Ishihara, Prediction of frequency distribution of strong crosswind in a control section for train operations by using onsite measurement and numerical simulation, Journal of Wind Engineering and Industrial Aerodynamics, Volume 174, pp. 69-79, 2018
35. Oriol Pons, Albert de la Fuente, Jaume Armengou, Antonio Aguado, Towards the sustainability in the design of wind towers, Energy Procedia, Volume 115, pp. 41-49, 2017
36. Takaaki FUKUHARA, Saki TANIMOTO, Keiji ARAKI, Methods to Estimate Spatial Distribution of Local Meteorological Conditions along Railway Line, Quarterly Report of RTRI, 2016, Volume 57, Issue 4, pp. 268-274, 2016
37. Keiji ARAKI, Takaaki FUKUHARA, Taisuke SHIMAMURA, Toshiaki IMAI, Method for Detecting Railway Line Sections Exposed to Strong Winds Using Numerical Simulations, Quarterly Report of RTRI, 2011, Volume 52, Issue 1, pp. 27-33, 2011
38. M. Burlando, A. Freda, C.F. Ratto, G. Solari, A pilot study of the wind speed along the Rome–Naples HS/HC railway line. Part 1—Numerical modelling and wind simulations, Journal of Wind Engineering and Industrial Aerodynamics, Volume 98, Issues 8–9, pp. 392-403, 2010
39. A. Freda, G. Solari, A pilot study of the wind speed along the Rome–Naples HS/HC railway line.: Part 2—Probabilistic analyses and methodology assessment, Journal of Wind Engineering and Industrial Aerodynamics, Volume 98, Issues 8–9, pp. 404-416, 2010
40. Tetsuya TAKEMI, Kenichi KUSUNOKI, Keiji ARAKI, Toshiaki IMAI, Kotaro BESSHO, Shunsuke HOSHINO, Syugo HAYASHI, Representation and Localization of Gusty Winds Induced by Misocyclones with a High-Resolution Meteorological Modeling, Theoretical and Applied Mechanics Japan, Vol. 58, pp. 121-130, 2010
41. W. H. Snyder, Experiments on Stably and Neutrally Stratified Flow over a Model Three-dimensional Hill, J. C. R. Hunt and Journal of Fluid Mechanics 96(04), pp.671-704, 1980